Tectonophysics 766 (2019) 1–13

Contents lists available at ScienceDirect

Tectonophysics

journal homepage: www.elsevier.com/locate/tecto

A 3-D structural model of the Saddle Mountains, Yakima Fold Province, Washington, USA: Implications for Late Tertiary tectonic evolution of the Columbia River Flood Basalt Province

Kelsey T. Crane*,[1], Christian Klimczak

Structural Geology and Geomechanics Group, Department of Geology, University of Georgia, Athens, GA 30602, USA

ARTICLE INFO

Keywords:
Yakima Fold Province
Fault
Fold
Structural geology
Tectonics

ABSTRACT

The Yakima Fold Province (YFP) is a series of asymmetric, north-verging anticlines in the Columbia River Flood Basalt Province of south-central Washington. Ridges represent anticlinal folds produced by tectonically active thrust faults, and their proximity to the Hanford nuclear facility has motivated many studies on the timing and extent of Quaternary deformation within the folds; however, multiple generations of faults and folds in the region have recorded a history of deformation spanning ~50 Ma. In this work, we utilize ~44 km of seismic profiles, structural orientation measurements collected in the field, USGS geologic maps, and stratigraphic information collected from 13 well logs to investigate the subsurface structure of the Saddle Mountains in the northern section of the YFP. We developed a three-dimensional structural model of the mountain range and estimated displacement and strain accommodated by faulting and folding. Our resulting model requires a multi-stage deformational sequence, and indicates that ~1800 m of uplift is generated by two parallel listric faults, soling into décollements at ~4 and ~8 km depth. Patterns of displacement and orientations of strain suggest that the deeper fault is older and that it may reflect a history of clockwise rotation, making the YFP the shortening counterpart to the extensional northern Basin and Range. The model presented has implications for understanding deformation in flood basalt provinces more broadly, and the methodology can be applied to interpret multi-stage deformation and reactivation histories of long-lived fault systems.

1. Introduction

The Yakima Fold Province (YFP) is a series of sub-parallel, mostly north-verging, asymmetric anticlines in the Columbia River Flood Basalt Province of south-central Washington. The mostly east – west striking fold system lies within the western Columbia Basin, bounded to the east by the Palouse Slope and to the west by the Cascade Range (Swanson et al., 1980). Today, the YFP is cut by the Columbia and Yakima Rivers. Rock uplift is accommodated through anticlinal folding and thrust faulting. Exposures of these structures as well as gravity, magnetic, well, geochronologic, and limited seismic data have supported our understanding of the fault geometry and timing of rock uplift (e.g. Reidel, 1984; Blakely et al., 2011; Casale and Pratt, 2015; Kelsey et al., 2017).

The east – west striking anticlinal ridges suggest north – south oriented shortening and maximum horizontal compressive stresses that have been attributed to Oregon Coast Block deformation during clockwise rotation within the North American Plate relative to the obliquely subducting Juan de Fuca Plate (e.g. McCaffrey et al., 2016; Unruh and Humphrey, 2017). Block motion models predict an Euler pole in northeastern Washington (Brocher et al., 2017) or the tri-state region of Washington, Idaho, and Oregon (McCaffrey et al., 2016; Unruh and Humphrey, 2017). These Euler Pole locations are derived from GPS measurements and structural analyses and predict that stresses and deformation increase to the west and structures align radially from the pole (Unruh and Humphrey, 2017). The block rotation models do not fully explain many of the anticlines within the YFP, such that more recently, a conceptual model proposing a slab tear along the Cascadia subduction zone and onset of asthenospheric flow has been invoked as an explanation for more recent north–south oriented compressive stresses (Staisch et al., 2017).

Block rotation models suggest that stresses began to build up ~15–16 Ma ago (Wells and McCaffrey, 2013; McCaffrey et al., 2013, 2016), approximately coeval with the initiation of basalt emplacement.

* Corresponding author.
E-mail address: kelsey.crane@uga.edu (K.T. Crane).
[1] Now at: Department of Geosciences, Mississippi State University, Mississippi State, MS 39762, USA.

https://doi.org/10.1016/j.tecto.2019.05.015
Received 21 January 2019; Received in revised form 8 May 2019; Accepted 21 May 2019
Available online 01 June 2019

Field studies suggest that deformation was coincident with the flow emplacement ~16 Ma (e.g. Reidel, 1984). Geochronologic studies of alluvial fans and strath terraces adjacent to the ridges propose that the majority of deformation occurred less than ~10 Ma ago, with fastest rates of uplift starting ~6 Ma ago (Kelsey et al., 2017; Staisch et al., 2017, 2018).

Structural analyses previously treated anticlines in isolation and in sequence to describe the faults and folds responsible for uplift. Cross sections derived from gravity and magnetic data and geologic maps indicate that thrust faults below the ridges extend ~8 km into basement rocks (e.g. Blakely et al., 2011; Staisch et al., 2018). Fault geometries range from smooth, arcuate fault surfaces dipping ~40°S with multiple branching conjugate thrusts (Blakely et al., 2011) to ~30° ramps interrupted by ~6 km wide flats at ~4 km depth (Staisch et al., 2018). Casale and Pratt (2015) infer from seismic data that two sub-parallel listric faults may form the ridges, with the more near-surface listric soling into a décollement below the southern slope of a ridge at ~4 km depth. The deeper fault in this two-fault model extends to a décollement at ~8 km depth. Field and modeling studies comparing folds of basalts to faults propagating through the flows also suggest deep structures (e.g. Campbell, 1989; Pratt, 2012). Conjugate thrust faults are commonly described, and fold geometry has been described as open to tight along the anticlines with folds occasionally displaying overturned limbs adjacent to thrust fault exposures (Reidel, 1984).

Our work links and expands on studies of uplift geometry and timing by developing a three-dimensional (3D) model of folded basalts and their associated faults before erosion. We interpret a dynamic, multi-stage evolution of folding and describe the relative timing and amount of uplift associated with a ridge using over 44 km of seismic profiles, well data, geologic maps, and field data. Understanding the cause and timing of uplift and the structural geometry allows for predicting modern earthquake frequencies and magnitudes. This is critical for the YFP. The Hanford Nuclear Site is located near several tectonically active Quaternary Yakima folds and the province may be structurally connected to a regional-scale mostly blind strike-slip structure, the Olympic-Wallowa Lineament that extends below the Seattle area and into the Puget Sound (Blakely et al., 2011; Pratt, 2012; Sherrod et al., 2016). Structural details also permit us to evaluate the regional tectonic context of the Cenozoic Pacific Northwest through a lens of the deformational record within the Yakima folds.

Characterizing structural geometry also provides key insight into deformational processes in flood basalts, making the Yakima folds a useful analogue for folds observed in basalts around the world and on other planetary bodies (e.g., Crane and Klimczak, 2019). Deformational processes may be long-lived, producing well-developed and complex fault networks. Our work serves as an example of how 3D modeling techniques can be used in conjunction with fieldwork to understand histories of deformation and reactivation and how to more broadly connect observed patterns in reactivation to evolving tectonic settings.

2. Methods

Our primary goal is to interpret the history of deformation within the YFP. We illuminated specific details of structural development by generating a 3D model of faults and folds with displacement and strain visualized on these surfaces. We chose to analyze the structure of a ~65 km length of the Saddle Mountains (Fig. 1) within the YFP based on availability of migrated seismic data and outcrop accessibility. The 3D model was developed by interpolating structures across 10 cross sections produced from field, seismic, well, and geologic map data.

2.1. Fieldwork

The Saddle Mountains is a ~110 km long segmented, north-verging anticline in the northern YFP. The ridge is cut by the Columbia River near Beverly, WA. East of the river, mass wasting events and drainage channel development have exposed basalt outcrop along the east – west striking anticline. West of the river, the anticline trends east – southeast and outcrop is exposed by mass wasting events and road cuts. The westernmost part of the Saddle Mountains is deflected northwest. To the south, the Manastash Ridge continues east – southeast toward the Yakima River.

Three primary Columbia River Basalt members are exposed in the Saddle Mountains: the Grande Ronde Basalts (16 Ma–15.6 Ma), the Wanapum Basalts (15.6–15 Ma), and the Saddle Mountains Basalts (15.0–6 Ma; Reidel et al., 2013). Each member is comprised of chemically distinct flows described in the literature (e.g. Swanson et al., 1979). Sedimentary interbeds representing pauses in volcanism separate some flows and support identification of flow units in the field. Descriptions of a few distinct flows and sedimentary interbeds make it possible to identify the member given context from geologic maps. For example, Grande Ronde Basalts form the thickest sequences of flows, and are capped by the very light-colored sedimentary Vantage Member of the Ellensburg Formation (Reidel and Tolan, 2013). The Roza Member of the Wanapum Basalts has 2–5 mm long plagioclase phenocrysts in parts of the flow distinguishing it from other Wanapum flows and is separated from the Priest Rapids Member of the Wanapum Basalts by the Quincy diatomite deposits (Tolan et al., 2009).

We traversed the Saddle Mountains and collected orientation measurements of planes inferred to have been horizontal during basalt emplacement (Fig. 2). These surfaces include sedimentary interbeds and upper contacts between sedimentary or ash layers and basalt flows. We also measured orientations of vesicle layers, major contrasts between sections of flows, flow tops, and planes perpendicular to well-developed colonnade and parallel to the long axis of oblate basalt pillows (see in Fig. 2: Aubele et al., 1988; Reidel et al., 2003; Sheth, 2018). No assumptions were made about the original horizontality for flow bottoms, as these may have been emplaced atop pre-existing topography.

We collected a total of 384 measurements using Midland Valley's *Clino* application for smartphones. The location of the measurements is shown in Fig. 1B, the measurements are provided as *.kmz files in the supplementary material. This *Clino* application is a digital geological compass and records georeferenced measurements and photographs that can be exported directly to the associated software modeling package *Move* or Google Earth. Each measurement was recorded with the basalt member in which it was collected and the type of surface it was taken upon. We also took 300 geo-referenced photographs (provided in the supplementary *.kmz files), and recorded hundreds of field observations and sketched the geometry of the folds where exposed. The Washington Division of Geology and Earth Resources smartphone application *Washington Geology* was also utilized in the field. The application allowed us to compare our orientation measurements in real time with previously collected measurements from published geologic maps. Where our orientation measurements differed substantially from the published data, we took additional measurements to increase our confidence in our interpretation. For example, on the western side of the Columbia River near cross section S6, the 1:24,000 geologic map (Washington Geological Survey, 2017) indicates vertical bedding. From a distance, these units do indeed appear vertical, but upon inspecting the outcrop, we observed that these units only appeared vertical, but were actually only slightly dipping. A differential weathering pattern had affected their ability to be interpreted from a distance (Fig. 3). For most measurements, our measurement was very similar to the published measurement, and because our dataset was more extensive than the available data, we chose not to utilize previously published basalt orientation measurements.

2.2. Seismic interpretation and wells

We obtained and interpreted four migrated seismic profiles. Three profiles cross the Saddle Mountains—two transect the mountains east of

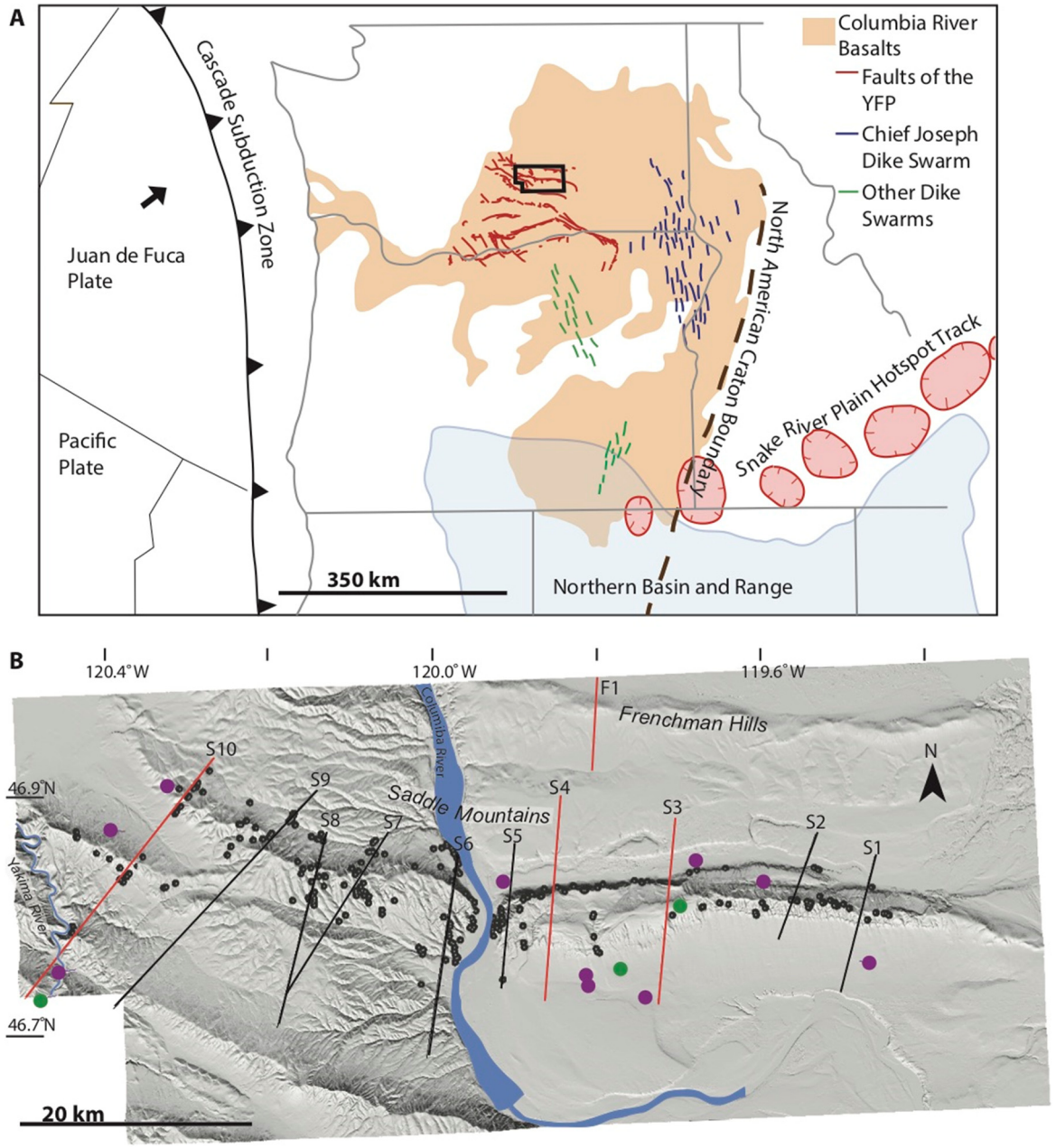

Fig. 1. Map of the Pacific Northwest for regional tectonic and volcanic context (A) and hillshade map of our study area highlighting the Saddle Mountains (B, produced from United States Geological Survey (2010) 10m DEM). The northern extent of the Columbia River Flood Basalt Province is shown in tan and Quaternary faults are displayed in crimson (United States Geological Survey, 2006). On the hillshade, black lines indicate cross sections without seismic profiles, and red lines indicate cross sections that contain seismic profiles. Sections S1–S10 cross the Saddle Mountains and are shown in Fig. 5 and available in more detail in the supplementary materials. Section F1 crosses the Frenchman Hills. Only structure was interpreted for this section, and it is not included in our 3D model. Purple and green circles represent respective locations of shallow and deep wells that provided stratigraphic information for cross section construction. Small black circles atop the hillshade represent locations of orientation data collected in the field. A more detailed map with strike and dip symbology and field photos is available in the supplementary materials, and can be directly opened in Google Earth for viewing. Context map displays regional tectonic and volcanic features such as boundaries for the Juan de Fuca Plate, Cascade Subduction Zone, Northern Basin and Range, and North American Craton (adapted from Camp, 2013 and Staisch et al., 2018). (For interpretation of the references to color in this figure legend, the reader is referred to the web version of this article.)

the Columbia River (S3 and S4) and one crosses the mountains west of the Columbia River (S10). The fourth profile crosses the Frenchman Hills (F1), the ridge directly north of the eastern section of the Saddle Mountains (Fig. 1B). Profile lengths are 9.5 km, 18.7 km, 11.5 km, and 14 km. For comparison, Casale and Pratt (2015) previously interpreted a ~22 km seismic profile near S5. Profiles along S3, S4, and F1 were produced by Arco Oil and Gas Company using Vibroseis equipment and shot intervals of 75 ft. They were filtered using low pass, Automatic Gain Control (AGC), and Normal Move Out (NMO) filters, and were migrated using post-stacking finite difference (30-degree) methods. The profile along S10 was produced by Shell Western E&P, Inc. using dynamite and shot intervals of 75 ft. Data was filtered using low and high pass, AGC, and NMO filters, and was migrated using a post-stacking Kirchhoff migration. Seismic Exchange, Inc. provided the propriety migrated profiles and Society of Exploration Geophysicists (SGY) format files. The software was used to visualize the SGY files and convert vertical time axes to depth, a conversion process which the software can also complete using the Root-Mean-Square (RMS)

Fig. 2. Field photographs exemplifying exposures and surfaces upon which orientation measurements were collected during fieldwork. (A) This westward view of the western Saddle Mountains highlights a broad exposure of folded basalts above the Columbia River. Folded basalts appear to drape horizontal strata; however, this is an effect of the perspective at which the photo was taken. Tilted well-developed columnar basalts (B and C) were also used to inform our cross sections as planes perpendicular to their surfaces indicate the amount of rotation that has taken place. The tilt or dip of these planes is symbolized with an arrow. Similarly, oblate pillows (D) which were emplaced with the widest dimension oriented horizontally were used to determine the dip of the basalt strata.

velocities provided in the Arco profiles. Each of the seismic profiles extends to ~9 km depth. We also used the *Move* software to interpret the profiles.

We identified faults, folds, and specific strata within the seismic data. The upper 200 m of reflections were difficult to interpret due to the multitude of fractures and discontinuous reflections. Below a few hundred meters, interpretation was based on continuity, amplitude, and spatial relationships of reflections. Folds were identified by arcuate reflections, and faults were identified by offset reflections. Horizontal reflections adjacent to tilted reflections were interpreted to be

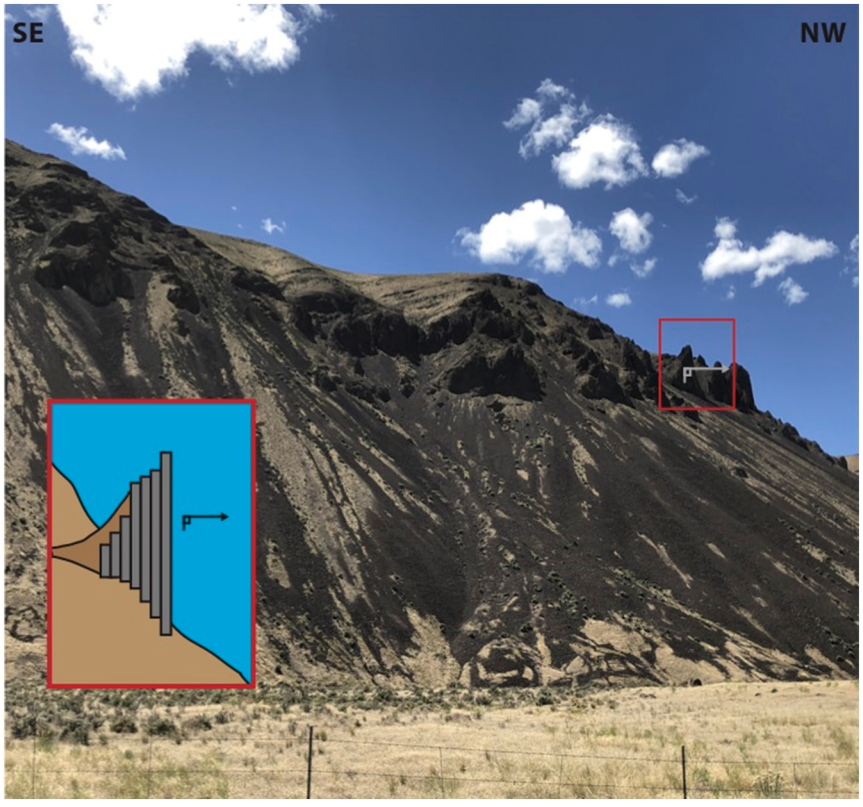

Fig. 3. This figure shows a photo of the northern slope of the Saddle Mountains just west of the Columbia River (fence for scale) and an inset digitized field sketch. The dark basalt units appear to be vertically oriented spires from a distance, but closer observation shows that the upward jutting rock is actually nearly horizontally oriented columnar basalt that has weathered into fin-shaped outcrops.

undeformed footwall strata juxtaposed to tilted hanging wall strata. A combination of water well logs and oil and gas well logs (Fig. 1B, purple and green circles) provided stratigraphic information that allowed us to tie our seismic reflections to specific basalt flows.

In particular, five oil and gas wells contained specific stratigraphic information. We used this information to directly link specific basalt members with reflection characteristics and indirectly link rock descriptions from shallower nearby water wells to named units in the oil and gas wells. For example, a ~1456 m deep well drilled by Boyles Bros. with identified stratigraphy provided constraints for classifying rock units in a ~342 m deep nearby water well. Units in the water well log were also described in detail by the drillers. A combination of rock descriptions from the drillers and approximate depths from the Boyles Bros. well allowed us to interpret the stratigraphy of the drillers log. Ten water wells less than ~1 km deep allowed us to constrain the depths of surface units and distinguish boundaries between flows using rock descriptions in the well log. All wells were located using the Geologic Information Portal of the Washington State Department of Natural Resources, and locations, depths, drilling information, stratigraphic tables, and direct links to well logs are provided for each well in the supplementary material.

Four oil and gas wells contain stratigraphic information about rock units beneath the Columbia River Basalts. The Yakima Minerals Well 1–33 (Shell Oil Company, 1983) lists the Swauk Formation as the deepest unit. The Swauk Formation is primarily sub-quartzose sandstone dating to ~59–51 Ma (Tabor et al., 1984; Eddy et al., 2016) and may be up to 8 km thick (Eddy et al., 2016). Where the formation outcrops north and west of the Columbia River Basalts, it has been observed to be folded and unconformably overlain by the relatively undeformed Teanaway Formation of basalt and andesite (~47 Ma) and Roslyn Formation (~45.9 Ma, Tabor et al., 1984). The Roslyn Formation consists of thickly-bedded sandstones interbedded with coals and siltstones (Tabor et al., 1984), and is observed in four of the oil and gas well logs, including the Yakima Minerals Well 1-33, BN1-9 (Shell Western E&P, Inc., 1984), AF1-6 (Delta Petroleum Corporation, 2006), and 23-35BN (Meridian Oil, Inc., 1988). Above the Roslyn Formation, the ~33–34 Ma Wenatchee Formation consists of volcanic tuff and is recorded in the BN1-9 and AF1-6 wells. The BN1-9 and AF1-6 wells align with our seismic profile along cross section S3, and Yakima Minerals Well 1-33 and 23-35BN are located along cross section S10. We characterized the seismic reflection of the Roslyn and Swauk Formations, and were therefore able to interpret their location on the seismic profiles in sections S3, S4, and S10. In these cross sections, we observed patterns of deformation within these deeper units reflected in upper units and surface structural geometries. We were thus able to extend our interpretations of formation surfaces to other cross sections. The seismic reflections associated with the Wenatchee Formation were so discontinuous that we did not feel confident interpreting the unit across the available seismic data.

2.3. Model development

We used Midland Valley's *Move* Software to generate our 3D model of structures within the Saddle Mountains. *Move* and similar structural geology modeling software packages allow for calculating and visualizing deformation-related parameters, especially where fault parameters vary over the study area (e.g. Bigi et al., 2013; Perrouty et al., 2014; Watkins et al., 2014; Muir, 2017; Linnros et al., 2019). *Move* allows the user to import, display, and manipulate shapefiles and field data collected with *Clino* in its graphical user interface. We imported a regional 10 m Digital Elevation Model and generated a hillshade. Two geologic maps (Reidel, 1988; Schuster, 1994) containing contacts, faults, and folds at 1:100,000 and 1:24,000 scales were loaded into *Move* followed by the structural data that we collected in the field. Field data and map information of geologic contacts, faults, and folds were projected onto the hillshade.

The combination of field data, mapped surface geology, seismic sections, and wells allowed us to construct 10 line-balanced cross sections of the Saddle Mountains (S1–S10, Fig. 1B). Details on observations and interpretations are provided with each cross-section in the supplementary material. *Move* contains functionality that allows the user to determine optimal cross section orientations based on imported data. The orientation data near the desired location of the cross section are plotted on a stereonet, and the plane most nearly perpendicular to the strike measurement is chosen. Field data were used to determine the orientations and locations of seven cross sections, while remaining sections are coincident with seismic profiles and near deep oil and gas wells. Structural field data and wells were projected onto cross sections within ~5 km of the data location. Data within ~5 km of cross sections but which clearly would not reflect the structures within that section were not projected. For example, data points collected in the east − west striking segment of the mountains were not projected onto profiles in the east − southeast striking segment. Topography and intersection points of contacts and structures from geologic maps were captured along cross section lines.

For cross sections containing seismic interpretations, strong reflections, strata defined by wells, and faults were identified first. Although the Frenchman Hills seismic profile was not included in the model, it was interpreted to provide additional context for the model (F1, Supplementary material). Any fault visible in the seismic data but not breaking the surface was noted, and folds visible at the surface associated with those blind faults were identified. If these folds extended across other cross sections, the fault was inferred to transect these sections as well. Line-balanced cross sections were then constructed using well data, structural field measurements, and surface geology. As previously described, stratigraphy available in well logs allowed us to characterize the flow units based on the visual properties of their seismic reflections. For example, the upper portion of the Roslyn Formation was characterized by three to four high amplitude, continuous reflections, and the Swauk Formation was characterized by many folds along the lower portions of the seismic profiles. We used a surface creation tool within *Move* to interpolate the top of the Grande Ronde flows, tops of the Priest Rapids and Frenchman Springs Wanapum flows, and major faults observed across the sections. We then described the geometry of the faults, calculating their length, depth, shape, and range of dips. We observed the geometry of the folds associated with faults. For specific descriptions of each of the cross sections, the reader is referred to the supplementary text.

2.4. Displacement and strain analysis

Faults and their associated folds evolve together over time. As faults grow in length, displacement along fault surfaces increases, with maximum displacement predicted at the midpoint of the fault length (Cowie and Scholz, 1992). Layer parallel shortening and flat-ramp fault geometry result in anticlinal folding above the upper fault edge, known as fault-propagation folding (Storti et al., 1997). Fault slip and associated strain is transferred into fault-propagation folds. Flat-ramp-flat fault geometries result in fault-bend folding. Fault-bend folds consume fault slip primarily near kinks in fault geometry, not necessarily along the upper fault edge (Suppe, 1983). Displacements accommodated by faults and folding are intimately tied to one another, and both must be evaluated to produce a complete model for deformational history.

We used the model described above and *Move*'s Geomechanical Modeling Package to calculate deformation-related parameters for the Saddle Mountains. The Geomechanical Modeling Package applies mass-spring algorithm, an iterative numerical technique, to minimize the strain in a solid body of rock, and then compares the strained and strain-removed surfaces to calculate strain-related parameters (Terzopoulous et al., 1987; Provot, 1995; Baraff and Witkin, 1998; Wang et al., 2006). We calculated the horizontal and vertical displacement, or heave and throw respectively, on the faults by defining

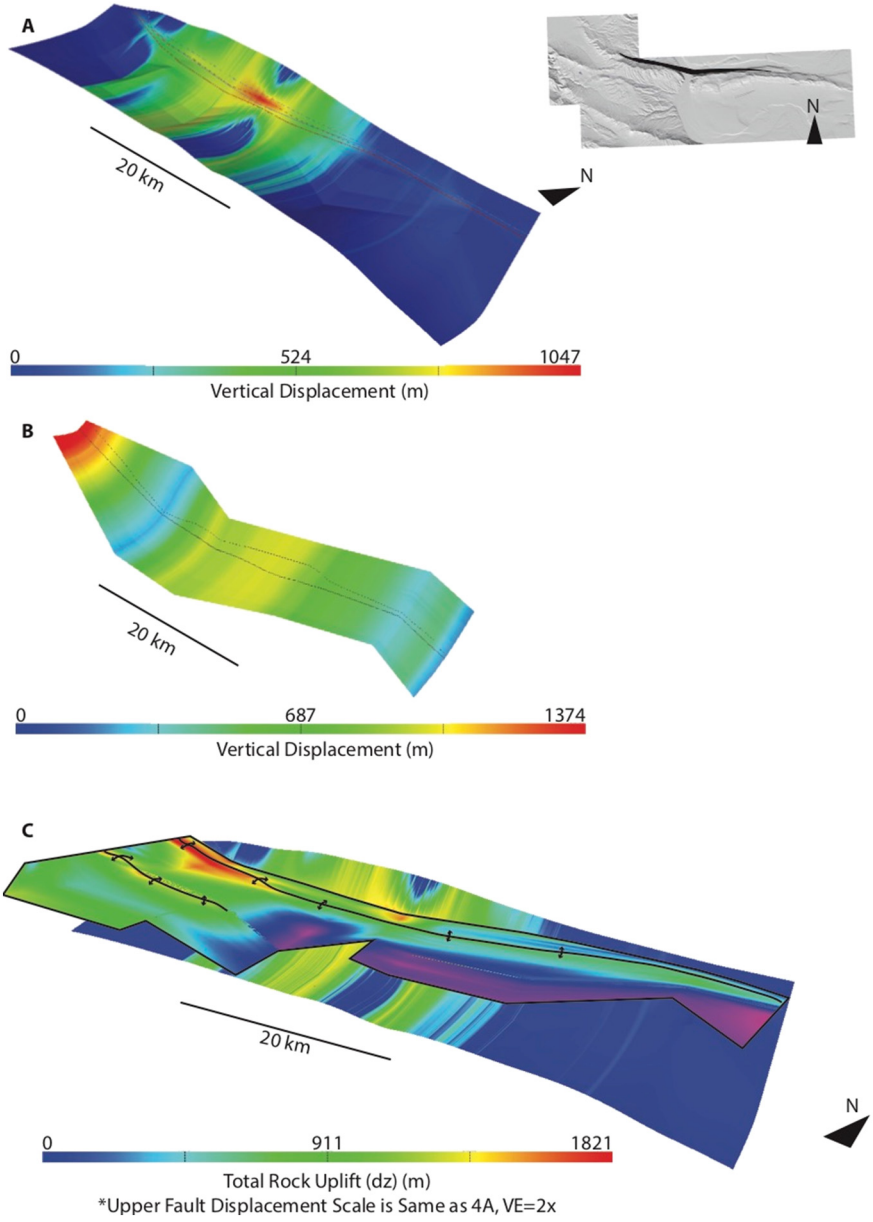

Fig. 4. This figure shows reconstructed surfaces of faults and one folded basalt layer, with warmer colors indicating greater amounts of vertical displacement. For spatial context, a small hillshade of the study area is provided, and the surface breaking portion of the major upper fault is shown in black. (A) The major upper thrust fault displays a pattern of increased vertical displacement near its center, just west of the Columbia River. (B) The deeper major thrust fault also has a minor peak in displacement near this location, but overall displays increased vertical displacement to the west. Faint black lines indicate identified hanging wall and footwall cutoffs. (C) The reconstructed Grande Ronde horizon is plotted with coloration indicating total rock uplift, and anticline symbology to indicate major anticline hinge zones. The maximum vertical change on this surface does not align with the maximum vertical displacement on the upper fault. The maximum vertical change in this unit more closely reflects the vertical displacement on the deeper fault. (For interpretation of the references to color in this figure legend, the reader is referred to the web version of this article.)

the intersections of hanging wall and footwall strata with faults and determining the distance between these intersections. We were also able to retro-deform or "unfold and un-slip" the reconstructed surfaces of the Grande Ronde and Wanapum Columbia River Basalt flows, and therefore calculate strain, strain direction, and total rock uplift. We differentiate the amount of deformation accommodated by faulting and folding. Because rock uplift is caused by folding and slip along thrust faults, subtracting vertical displacement due to faulting from total rock uplift discerns uplift or elevation change caused by folding alone. We mapped these values across the surfaces of the faults and folds to detect patterns in location or intensity of deformation.

3. Results

3.1. Structural geometry

The series of cross sections reveals a 3D structural system of listric thrust faults, conjugate thrust faults, and varied folds (Fig. 4). The main frontal thrust below the Saddle Mountains (Fig. 4A) is often interpreted to break the surface (e.g. Reidel, 1988). We observe this listric thrust fault in seismic profiles to extend to ~4 km depth (4.4 km at the deepest) before soling into a décollement within the sedimentary Roslyn Formation. We recognize this fault due to offset reflections extending toward the mapped surface break. The main frontal thrust fault produces the major displacement due to faulting of the Columbia River Basalt units and minor displacement due to faulting of the Roslyn Formation. This fault spans the entire length of our model (~65 km), and likely extends tens of km beyond the model boundary. Where the fault breaks the surface, the listric geometry is characterized by dips primarily between 32°S and 53°S, with a steepest dip of 66.5°S. These dips are taken directly from the model which is constrained by dips calculated from strike lines of surface-breaking sections of the fault on the geologic maps.

A second major thrust (Fig. 4B) is also observed in seismic data, but is not mapped at the surface. This fault is evidenced by offset reflections at and near ~7.5 km depth and subsurface, north-verging folds. Offset dissipates stratigraphically upward until ~4–4.5 km where the fault and folds are capped by sub-horizontal strata which may be lower Roslyn Formation (~45.9 Ma) or basalts of the Teanaway Formation (45–47 Ma). This deeper fault is interpreted to propagate toward the

surface in some sections, and its upper edge is located below an open anticline north of the main anticline. The long-wavelength fold morphology of the entire anticline consists of a general upward bowing of the topography and is observed in many of the cross sections. The arch of this fold directly overlies the deeper fault. The fault extends the length of the model, with most dips between 31°S and 51°S and a maximum dip of 70°S. The two main thrusts are parallel. This system of two main faults beneath a anticline is also observed in the Frenchman Hills seismic profile (F1, Supplementary materials).

We also identify two minor faults in seismic profiles. These faults are also present in geologic maps. A backthrust in the easternmost region of our model dips approximately 40°N, rooting into the upper listric thrust. This fault slightly shallows with depth, and extends to ~2.4 km depth. The modeled length is ~21.6 km; however, the fault likely extends a few hundred meters beyond the modeled boundaries. While this fault does not break the surface, the southernmost extent of the fault is located directly beneath a southward verging mapped anticline. A second conjugate fault located in the western region of our model does break the surface. This fault is currently mapped as two faults; however, we interpret a single fault with changing dip based on surface geometry of mapped folds and faults. The eastern portion of the fault dips ~45°S. It dips more shallowly near its length midpoint (~15°S) and steepens to ~45°N in the west as the fault transitions to dipping north. It is ~30.7 km long, and extends to ~1.9 km depth.

Folding style is variable along the length of the Saddle Mountains. Folds were observed by analyzing field photos (included in supplementary *.kmz file), sketches and shapes of reconstructed flow surfaces within the larger Grande Ronde, Wanapum, and Saddle Mountains Columbia River Basalts units. In the easternmost study area, we observe open box folds. Fold axial traces align with upper fault edges for the main fault and backthrust. In particular, a south-verging fold above the eastern backthrust is prevalent in S1–S3. Farther westward toward the Columbia River, folds transition into short-wavelength structures (less than ~2 km) superimposed on a broader, anticlinal structure (tens of km in wavelength, Fig. 5, S3 and S4). Deeper folds associated with the lower listric thrust fault mimic this long-wavelength structure.

Immediately west of the Columbia River, folding style abruptly changes. A north-verging anticline dominates above the upper listric thrust fault with lower-wavelength folds overlying kinks in the fault ramp (Fig. 5, S6 and S8). The longer-wavelength structure of the fold mimics the transition from the ramp into a décollement at ~4 km as well as the geometry of the deeper thrust (Fig. 5, S6 and S10). A north-verging open anticline overlies a minor thrust south of the major, upper thrust and is trailed by a long-wavelength syncline. Minor synclines are observed south of the main thrust fault superposed on the larger anticlinal structure. As the upper fault edge drops below the surface in the westernmost region of our study area, the main anticlinal fold becomes more symmetrical, and the steepening, conjugate minor thrust fault produces a more exaggerated south-verging fold (Fig. 5, S10). South of this fold along cross section S10 another major north-verging anticline is present. The Umtanum Anticline is similar in scale to the Saddle Mountains Anticline. The structure of this separate anticline is not the focus of this work, so its presence is noted, but it is not analyzed completely within our model.

3.2. Displacement and strain

Faults accommodate a portion of the vertical displacement within the Saddle Mountains. Displacement on each of the major faults is visualized in Fig. 4 and shown in the displacement profiles in Fig. 5. The major, upper listric thrust (Fig. 4A) has a maximum vertical displacement of ~890 m, which occurs within the Grande Ronde member and decreases upward into the Wanapum Basalts. Specific values for vertical displacement along this and the deeper major fault are available in the supplementary materials. Displacement along the upper major thrust fault peaks near the Columbia River where the strike of the anticline shifts northwestward. Just east of the Columbia River, this fault displays a minor peak in vertical displacement of ~690 m. Two peaks in vertical displacement, one aligning directly below the eastern displacement peak of the upper listric thrust, also characterize the major, deeper listric thrust (Figs. 4B and 5). The distribution of displacement about this peak is more dispersed in the deeper fault than in the upper fault. The maximum vertical displacement on the major, deeper listric fault (~1360 m) is in the farthest westernmost study area, calculated from offset of seismic reflections possibly within the Swauk Formation near 6 km depth. Vertical displacement appears to taper upwards, where less offset between seismic reflections is observed and folding becomes more apparent (near 4.5 km depth).

Offset in the Grande Ronde and Wanapum members was used to calculate maximum vertical displacement along the two minor faults (displacement along these faults is shown in Fig. 5 and specific values for displacement and slip for each unit are provided in the supplementary materials). The maximum vertical displacement observed along the western, minor thrust fault is ~385 m and is located along the eastern reaches of the fault, just west of the Columbia River. The maximum vertical displacement along the backthrust in the eastern segment of the Saddle Mountains is ~106 m and is localized in the western reaches of the fault. In general, we observe little displacement along the faults in the easternmost region of our study area (Fig. 5).

Folding is primarily responsible for uplift in the eastern region of the Saddle Mountains (Table 1), and has produced large anticlines in the western region (Fig. 5, e.g. S10, Saddle Mountains Anticline). Orientations and structures within reconstructed flows were well constrained by field observations relative to older, deeper flows. Reconstructed surfaces reflect the shorter-wavelength folds associated with the upper, major thrust and the long-wavelength influence of the lower, major thrust (Fig. 4B). Anticline axial traces nearly overlie the near-surface fault edge of the major, upper thrust fault, suggesting that the style of folding is fault-propagation folding or fault-bend folding lacking a developed upper flat (Yan et al., 2016). In either case, the continued slip at the upper fault edge has been transferred into folds.

We calculate the total rock uplift to range from 35 m to 1821 m across the study area (Fig. 6). Using assessments of vertical displacement on the major, upper thrust surface, we estimate that folding and long wavelength rotation on the deeper fault are responsible for ~1539 m, ~656 m, and ~1043 m of vertical displacement in the far western region of our field area, the region surrounding the Columbia River, and the far eastern region of our field area, respectively (Table 1). In the central region of our study area, vertical displacement along the upper fault and vertical displacement on the lower fault together exceed the total rock uplift. We can therefore calculate displacement on the lower fault that is not expressed on the folded, reconstructed surface (253 m, Table 1). If all vertical displacement is consumed by faulting, then no total rock uplift is to be accounted for by folding; however, we observe folds throughout our study area. Thus, this “missing” displacement represents a minimum displacement on the deeper fault that is not expressed at the surface. If the deeper fault does not affect vertical displacement of the reconstructed surface, then all rock uplift not accounted for by the upper fault is due to folding. If all of the vertical displacement on the deeper fault is expressed at the surface, and the total rock uplift exceeds the vertical displacement on both faults, then the remainder of vertical displacement is due to folding alone.

Unaccounted for displacement on the deeper fault, 253 m near cross section S5, implies that at least 253 m of vertical displacement on this fault may also not be expressed in the reconstructed surface at other locations in our study area. We can therefore estimate that ~250 m of total rock uplift in these other locations is due to folding, not faulting, and shows us that our estimates for contribution of folding to total rock uplift are likely minimums. When accounting for the 253 m adjustment, faulting produces 1186 m, 1546, and 244 m of total rock uplift and folding produces 635 m, 0 m, and 846 m of total rock uplift in the

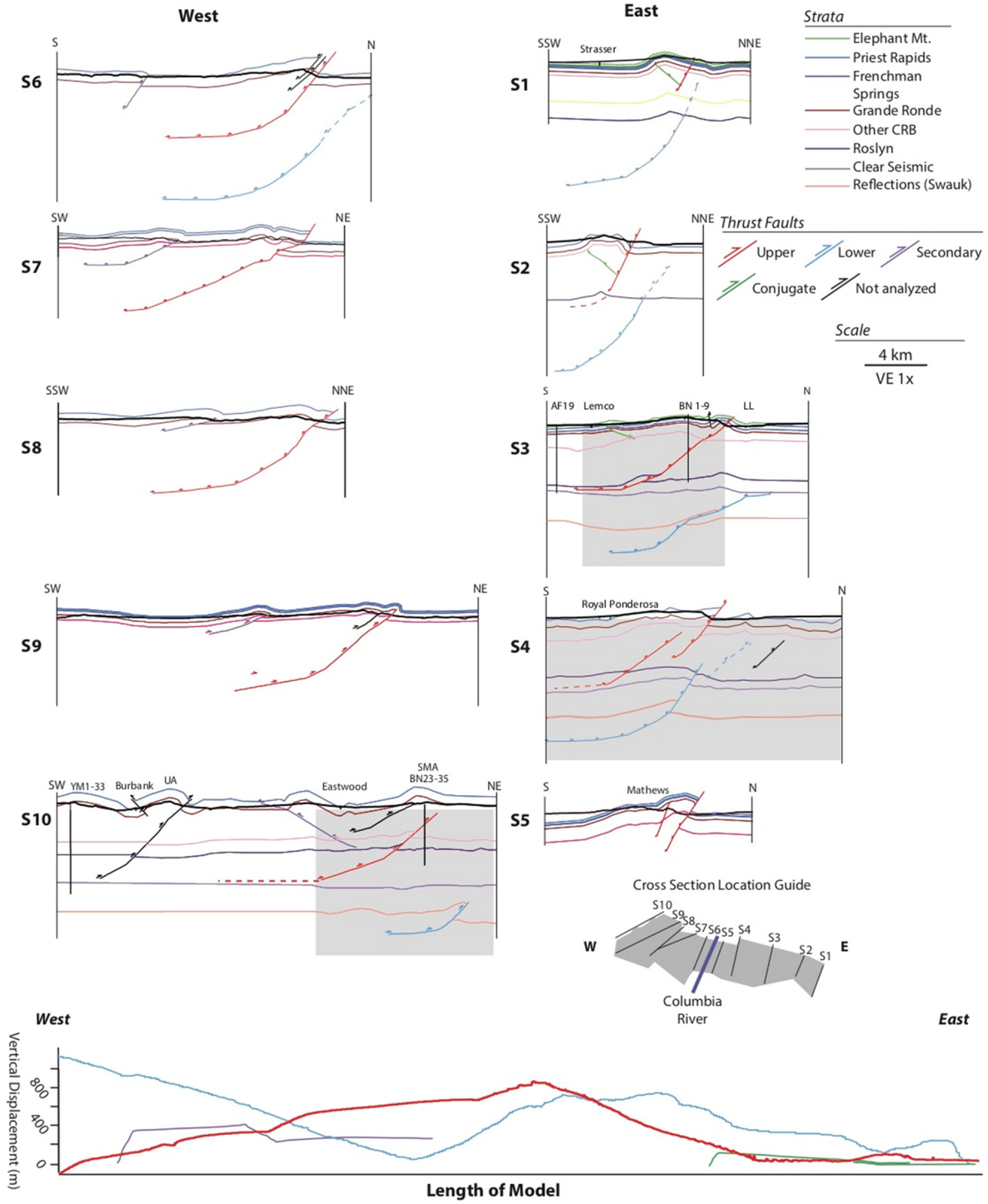

Fig. 5. This figure shows 10 cross sections (West of the Columbia River on left, East of the Columbia River on right). Cross sections correspond to lines shown in the Cross Section Location Guide (lower right). Strata colors vary for each of the flows identified in well data, seismic data, or geologic data. Black vertical lines indicate wells with stratigraphic information and gray shading corresponds to available seismic profiles. In S10, two major anticlines are present, Umtanum Anticline (UA) and Saddle Mountains Anticline (SMA). The Saddle Mountains Anticline is in the northern portion of the cross section and is the focus of this work. There is no vertical exaggeration, and all cross sections utilize the same scale. In the lower portion of the figure, we plot vertical displacement against the length of the study area from West (left) to East (right). Fault colors correspond to those in the cross sections. Peaks in displacement are visualized as maximums along these curves. All cross sections are available larger and in more detail in the supplementary text. (For interpretation of the references to color in this figure legend, the reader is referred to the web version of this article.)

western, central, and eastern Saddle Mountains (Table 1).

The east–west component of displacement is relatively consistent along the ridge, < 300 m along the anticline crests and southern slopes. Near the Columbia River where the anticline strike changes, east–west displacement estimates reach ~500 m.

Unfolding of the reconstructed flow surface was also used to calculate strain within the study area (Fig. 6). We investigated strain oriented purely north–south (S_{yy}), normal strain oriented in the direction of maximum horizontal shortening (S_3), and the azimuth of S_3. We chose these parameters because Yakima folds are typically described as

Table 1
This table displays estimates for total rock uplift and vertical displacement taken directly from the Grande Ronde reconstructed surface of our model and the intersection of this surface with the upper and deeper major faults. We use these values to estimate the contributions of faulting and folding to total rock uplift.

	West (near S9)	Central (near S5)	East (near S2)
Total rock uplift (m)	1821	1546	1090
Upper fault Vertical displacement (m)	282	890	47
Deeper fault Vertical displacement (m)	1157	909	450
Maximum vertical displacement expressed by deeper fault, and maximum rock uplift from folding alone (m) (Row 1 − Row 2)	1539	656	1043
Minimum rock uplift from folding alone (m) (Row 1 − Row 2 + Row 3)	382	0[a]	593
Folding contributions to rock uplift using "missing" 253 m vertical displacement from deeper fault in S5 (m) (Row 5 + 253 m)	635	0	846
Faulting contribution from both upper and deeper faults to rock uplift using "missing" 253 m vertical displacement from deeper fault in S5 (m) (Row 1 − Row 6)	1186	1546	244
Folding and faulting contributions to total rock uplift as % based on estimates in rows 6 and 7	35%/65%	0%/100%	78%/22%

[a] Mathematically, the result was −253 m; however, this value cannot physically be negative, so it must be zero.

north-verging—implying a north–south oriented maximum principal stress propagated from the south. Contrasting values and distributions of S_{yy} and S_3 within the study area illuminate which segments of the ridge conform to the traditional stress characterization. By measuring the azimuth of S_3, we can visualize the orientation of maximum principal stresses responsible for strain and uplift.

North–south oriented strain (S_{yy}) is concentrated in the eastern region of the Saddle Mountains (Fig. 6). West of the Columbia River, S_{yy} is greatest along the southern limbs of the folds, reaching 1.0% in most places. East of the Columbia River, S_{yy} is concentrated on the crests and southern limbs of the folds, but is greater in magnitude reaching, 8.0–13%. We also calculated shortening amount and percentage for each cross section. Values for shortening amount range from ~337 m in the east to ~1500 m in the west. Shortening percentages averaged ~5%, but again, increased from ~2.5% to 8% in the west.

In the eastern Saddle Mountains, S_{yy} and S_3 align; however, in the western Saddle Mountains, S_3 is oriented north–northeast. The majority of azimuths of S_3 range from 003° to 026°, with a mean and median of 022° and 014°. West of the Columbia River, azimuths primarily range from 020° to 030°. Like S_{yy}, S_3 is localized along the crests and southern limbs of the folds. In the west, values are between 1.0% and 8.0% in most places and in the east, values are between 1.0% and 13%. These strain values indicate the primary direction of shortening is north–south and north–northeast in the eastern and western study area, respectively.

4. Discussion

4.1. Parallel fault surfaces

The fault surfaces visualized in our model reveal unexpected geometries and stress the importance of décollements on this developing tectonic landscape. We observed a fault in the western Saddle Mountains that changed vergence and dip (purple fault, Fig. 5). In S10, this fault is steep and conjugate to the upper, main thrust. In S8–S9, it transitions to a south dipping thrust. The deep edge of this fault terminates near the top of the Roslyn formation which may have been utilized as a décollement horizon. Weak layers that encourage décollement formation may also promote faults which change vergence along strike (e.g. Higgins et al., 2007). The two major thrust faults may also root into décollements, as the seismic reflections indicate listric fault geometries and reflections in the hanging walls more distal from the faults appear sub-horizontal. The upper, major thrust is found to sole into the Roslyn Formation, as we did not observe offset seismic reflections associated with this fault below this formation. The fault may continue sub-horizontally within the Roslyn Formation or it may terminate within this stratum, but within our seismic window, we do not observe seismic reflections of the sub-horizontal strata above the lower folds to be offset by this fault. If this fault does plunge below the Roslyn Formation, it is not shown in our seismic data. Both faults are steeper than anticipated, and their parallel geometry is similar to one of the proposed geometries by Casale and Pratt (2015).

Many earthquakes within the YFP occur deeper than 5 km. Gomberg et al. (2012) found that only one-third to one-half of earthquakes in the YFP were focused within the Columbia River Flood Basalts. They observe peaks in seismicity at 1–5 km depth and 5–10 km depth. The vast majority of these earthquakes appeared uncorrelated to fault traces, fold axes, or other mapped structures. Our results suggest that these earthquakes, particularly those focused below 5 km, may be related to deep structures such as the lower, major thrust fault, and the depths characterized by seismicity correlate with activity along identified décollements.

The parallel surfaces of the two major faults are startlingly similar, but differences in fault depth and displacement motivate questions of when and why tectonic activity occurred along the two faults. We interpret from seismic profiles that the deeper thrust fault and its associated folds are capped by relatively horizontal to mildly folded units. Some smaller faults appear geometrically related to this deep fault, extending north of the upper fault edge, but these small faults are characterized by very little displacement of seismic reflections. The upper major thrust fault extends from the sub-horizontal strata upward toward the surface. That we do not observe the deeper thrust fault cutting through those sediments and do observe a strong geometric contrast between the pronounced anticlines associated with the lower thrust fault (after ~51 Ma, post-Swauk Formation) and the horizontal layers superposing those folds (possibly Roslyn Formation) implies a break in time between the development of folds above the lower fault and the initiation of the upper fault and Columbia River Basalt emplacement (~16 Ma). This is most apparent in S10 where exaggerated folds and large vertical displacements on the lower fault contrast with sub-horizontal strata (possibly belonging to the Swauk Formation) above. This pattern is not unique to the Saddle Mountains, and can be observed in the Frenchman Hills (F1 interpreted seismic section in the supplementary text). During the break in time between lessening of activity on the deeper major thrust and propagation of the upper major thrust (between ~52 Ma and ~16 Ma), a change in the deformational style of the deeper thrust may have occurred. Even as the upper, major thrust fault propagated to the surface, the lower fault may still have accommodated deformation. We interpret long-wavelength, upward folding mostly present in the western region of the study area to be caused by deformation along this deeper fault.

Contrasting displacement distributions on the fault surfaces imply

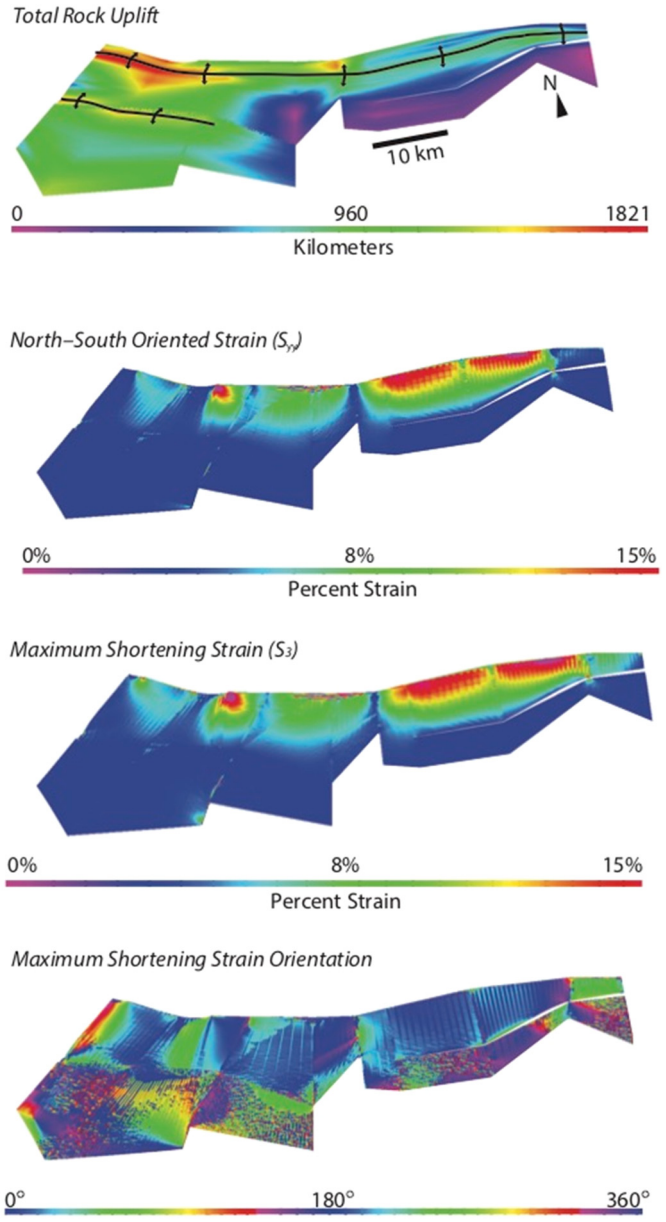

Fig. 6. This figure shows total rock uplift considering folding and vertical displacement from faulting, north–south oriented strain (S_{yy}), maximum shortening strain (S_3), and orientation of maximum shortening strain visualized on the unstrained or unfolded upper Grande Ronde flow surface. Anticline crests are mapped. North–south oriented shortening is greatest in the eastern Saddle Mountains, and maximum shortening in the western Saddle Mountains is aligned north–northeast–south–southwest.

differences in causes of deformation. The upper, major thrust has evolved as predicted by fault growth models (e.g. Cowie and Scholz, 1992). Maximum vertical displacement is located near the fault length midpoint and dissipates outward toward the fault tips (Figs. 4A and 5, displacement profile). The orientation of S_3 and agreement of S_3 and S_{yy} strain values indicate that north–south oriented maximum horizontal compressive stresses were responsible for the uplift along this fault. The lower major thrust, however, shows greater displacement to the west, with a secondary peak in displacement just east of the Columbia River. The alignment of this peak with a local maximum in the displacement on the upper, major thrust indicates that the lower fault reactivated during the evolution of the upper, major thrust fault. Increased vertical displacement on the lower, major thrust fault and long-wavelength topographic development associated with that fault toward the west imply that this fault propagated in response to clockwise rotation of crustal deformation. An eastern Euler pole and clockwise block motion produced increased westward deformation.

4.2. Local history of deformation

Our results show that the YFP has recorded a long and changing history of deformation in the Pacific Northwest. The distribution of displacement across the deeper, major thrust surface emphasizes the pattern of westward increasing strain and stresses. These stresses could have been caused by regional clockwise rotation within the North American crustal block. Strain was accommodated through anticlinal folds above the thrust fault after the deposition of the Swauk formation 59.9–49.9 Ma but before the deposition of the Roslyn Formation after 45.9 Ma (ages, Tabor et al., 1984; Cheney, 1994; Eddy et al., 2016). This estimate is consistent with the results of Eddy et al. (2016) which show that between 51.3 and 49.9 Ma west–northwest trending folding shortened the Swauk Formation. The Roslyn Formation caps the subhorizontal cover strata lying unconformably above the folds, implying a pause in deformation after 49.9 Ma. Increased stresses reinitiated deformation before or during the emplacement of the Columbia River Basalts. The increased topography in the west observed today indicates that even as the Columbia River Basalts were emplaced, strain continued to accumulate, rotating and vertically displacing the basalts and sub-basalt units. The fault was too deep to produce short-wavelength topography, and this inefficiency spurred the development of an upper, major thrust at the top of the mildly deformed sequence.

The upper, major thrust fault accommodated mostly north–south oriented stresses after ~16 Ma. The deeper fault experienced some reactivation due to this north–south oriented shortening, but the pattern of displacement on this fault is fundamentally different from the upper, major fault. The differing patterns in faults of two contrasting ages imply that the tectonic context and thus stress orientation must have evolved over time. This change in stress orientation postdated emplacement of the Columbia River Basalts, as all of the basalt units are cut by or folded above the upper fault. Continued clockwise rotation in modern times may still be accommodated by the deeper fault, accounting for the deep earthquake foci discussed above.

We interpret that there must have been a time of north-northeast–south-southwest oriented shortening before ~50 Ma, followed by a pause in deformation. Deformation resumed sometime before the emplacement of the Columbia River Basalts at ~16 Ma. After this time, stresses reoriented north–south and rock uplift continued in a context of ongoing clockwise block rotation. We relate these events to our field observations and to regional-scale volcanic and tectonic context of the Eocene Pacific Northwest.

4.3. Connections to regional tectonics and volcanism

Establishing a timeline for deformation and constraints on the direction and style of shortening has allowed us to hypothesize about tectonic influences on deformation. We connect the geologic histories of the Farallon and Juan de Fuca plates, the Chief Joseph Dike Swarm, Snake River Plain Hotspot Track, and the northern Basin and Range in a conceptual model to interpret the deformation preserved in the Yakima Folds and their structural predecessors (Fig. 1A). Each of these geologic phenomena has been connected to at least one of the others through extensive research, but because the YFP is so centrally located within the Pacific Northwest, we find that all components of this regional tectonic story are represented in its structures.

This history begins with the formation of the Siletz-Crescent terrane during the early Eocene (described by Snavely et al., 1968). Paleomagnetic reconstructions and block motion models show that prior to 55 Ma, the Farallon and Kula plates were rapidly and obliquely subducting below the western North American craton (e.g. Wells et al., 1984; McCrory and Wilson, 2013). The boundary between these two

plates was disturbed by a mantle plume. This rising plume triggered hotspot volcanism, producing thick, buoyant basalts with compositions reflective of the mantle source (Graham et al., 2009; Pyle et al., 2009; Chan et al., 2012; Wells et al., 2014). As the Farallon plate continued to subduct, these basalts were accreted onto the western North American craton (Duncan, 1982; Wells et al., 1984). The formation of the accreted terrane, now called the Siletz-Crescent terrane has been dated to 55–49 Ma (Duncan, 1982; Moothart, 1992; Wells et al., 1994, 2000).

Oblique, northeastward subduction of the Farallon plate, and its slab rollback, encouraged clockwise rotation of the accreted terranes (Simpson and Cox, 1977; Beck, 1980; Wells et al., 2000; McCrory and Wilson, 2013). The rigid craton, however, resisted rotation (Wells and McCaffrey, 2013), and behaved as a rotational axis for the continued clockwise crustal motion. Clockwise rotation about this axis would have produced extension southwest of the Euler pole and west of the craton boundary, and it would have produced shortening west of the Euler pole and craton boundary. Regionally, terranes more distal from the axis would have experienced more intense deformation than terranes closer to the axis, similar to the swinging of a door about a hinge. Far from the "hinge", the northern Basin and Range display evidence of clockwise rotation during this time. Wells and Heller (1988) estimated 33% extension for the northern Basin and Range from 37 Ma to 50 Ma. These authors also estimate 39% extension since 37 Ma and 17% extension since 15 Ma, similar estimates to the 40–50% extension estimated by Colgan and Henry (2009). This implies a long history of opening and rotation in the region continuing after the accretion of the Siletz-Crescent terrane.

We propose that the westward increase in deformation observed in the lower, major thrust fault recorded this clockwise deformation. To expand our door analogy, as the door was opening in the Basin and Range, it was closing in central Washington. This closing would have been expressed through folding and thrust faulting of the sedimentary and volcanic sequences present in the region. Nearer to the door hinge, the expected deformation in the YFP region would have much less than that recorded in the Basin and Range, ~5–10% compared to the ~40% cited above.

Clockwise rotation slowed as slab rollback decelerated and the Farallon slab detached from the Juan de Fuca Plate. Block motion models show that detachment of the Farallon slab and resultant slowing subduction of the Juan de Fuca Plate occurred ~52 Ma (Caress et al., 1988), similar to when Eddy et al. (2016) estimate north-northeast–south-southwest oriented shortening (49.9 Ma). A pause in rapid rotation after 49.9 coincides with the period of interpreted tectonic quiescence in the Saddle Mountains. Reduced tectonic activity resulted in the deposition of observed sedimentary layers, such as the Roslyn Formation, atop the folds associated with the deeper major thrust.

During this pause, a slab window opened that allowed for the eastern migration of the plume that had formed the Siletz-Crescent terrane (e.g. Obrebski et al., 2010). By 19–17 Ma, the Juan de Fuca Plate had resumed oblique, northeastward subduction (Wilson, 1988; Wells and McCaffrey, 2013). The associated clockwise rotation due to rollback reinitiated. The combination of an active mantle plume and a passive crust-mantle environment encouraged volcanism in Northwestern Nevada. Camp (2013) describes that as the plume continued eastward, the plume head was decapitated along the North American craton. While the plume head migrated northward along the craton boundary, near the western boundaries of Oregon and Washington, it produced northward propagating dikes (Camp and Ross, 2004). At ~16 Ma, in the opening stress conditions near the rotational axis, the Chief Joseph Dike Swarm released the main phase of the Columbia River Basalts (Reidel et al., 2013). Smaller opening stresses near the rotational axis explain the lack of extensional tectonics associated with the swarm. The tail of the plume continued eastward forming the Snake River Plain Hotspot Track, which again reflected the deep mantle source (Graham et al., 2009). To the south, the lack of plume activity contributed to a volcanically quiet Basin and Range opening.

Strain associated with the Chief Joseph Dike Swarm are < 1% (Camp, 2013; Morriss and Karlstom, 2018), similar in order of magnitude to the strain displayed in the Saddle Mountains, a section of their compressional counterpart, the YFP. During this time, broad, long-wavelength topography developed primarily in the western front of the Saddle Mountains along the deeper, major thrust. Coevally, a new fault—the upper, major thrust—began to propagate through the base of the Columbia River Basalts.

Tectonism waned after emplacement of the Grande Ronde flows, ~15 Ma, suggesting a reorientation of regional stresses. The transition to north–south oriented horizontal compressional stresses prompted the slowing of volcanism, rock uplift of the eastern Saddle Mountains, and development of shorter-wavelength folds across the entirety of the Saddle Mountains. Our cross sections show large displacements on the upper Saddle Mountains Basalts, and thus indicates that faulting must have been active after the emplacement of these members (~10 Ma, Reidel et al., 2013). Other studies also support that tectonic activity on the eastern segment of the mountains is recent, as modern as ~6 Ma (West et al., 1996; Staisch et al., 2018). During this time, the rate of convergence of the Juan de Fuca Plate with the North American Plate slowed, also reducing the speed of regional crustal clockwise rotation (Wells and McCaffrey, 2013). The north–south stresses may be indicative of toroidal flow above a torn, subducting Juan de Fuca Plate (Staisch et al., 2018 and references therein). This change in stresses and recent uplift is reflected in the displacement distribution of the upper major thrust and reactivation of the deeper major thrust.

5. Conclusions

We investigated the structural geometry and cause and timing of deformation for the Saddle Mountains, an anticline within the YFP. Fieldwork, seismic interpretation, and digital well and geologic data allowed us to construct a 3D model of the structures within the Saddle Mountains. This model proposes that two parallel listric thrust faults are responsible for the majority of topographic development along the ridge. The lower, major thrust fault and its associated folds recorded north–northeast–south–southwest oriented shortening prior to the emplacement of the Columbia River Basalts. Focused in the western Saddle Mountains, deformation along these structures continued after basalt emplacement, producing primarily long-wavelength topography. The upper, major thrust fault recorded more recent, north–south shortening that occurred after ~10 Ma. Folds that developed above this fault are responsible for short-wavelength topography. Parallel displacement across both faults in one region of our study area indicates that the lower fault may have been reactivated during more recent episodes of fault slip. All faults and folds record 2.5–13% strain.

Orientations and timing of this strain has allowed us to hypothesize how it may have accumulated. During the early Eocene, subduction, slab detachment, and plume activity generated a complex tectonic environment that spurred clockwise rotation within northwestern North America. This rotation was recorded in the Basin and Range and in structures beneath the present-day Yakima folds. Continued plume activity in the rotating crust generated the Columbia River Basalts, and more deformation within the folds. Reoriented stresses produced the younger north-verging folds we see today.

This work provides the basis for future research. Three-dimensional models with visualized displacement can be used to predict future seismic activity. They will also allow us to locate candidate field sites that are most likely to record kinematic indicators, such as deformed vesicles, facilitating future fieldwork. More work like this is necessary to address structural linkage between multiple folds within the YFP and to determine if parallel, listric faulting is a universal characteristic of the YFP. Our observation of deep structure and reactivation implies that there is certainly a connection between structures at multiple depths, and these structures may connect across Yakima folds. Understanding this linkage is critical for estimating seismic hazards (Last et al., 2012),

as large connected fault zones pose increased hazard potential, and for contextualizing the YFP within the larger regional tectonic setting.

Acknowledgements

We thank Dr. Lydia Staisch and Dr. Harvey Kelsey for helpful review of the manuscript and Seismic Exchange, Inc. for the use of seismic profiles. Authors also acknowledge the use of the IPM and/or MOVE Software Suite granted by the Petroleum Experts Limited. We also thank the Bureau of Land Management, US Army Corps of Engineers, Department of Natural Resources, Department of Fish and Wildlife, and US Bureau of Reclamation for access to public lands, and Mr. Gary Maughan for access to private property. Funding for research was provided by the University of Georgia Graduate School Summer Research Grant and Geology Department Allard and Watts Wheeler Awards.

Appendix A. Supplementary data

Supplementary data associated with this article can be found in the online version, at https://doi.org/10.1016/j.tecto.2019.05.015. These data include the Google maps of the most important areas described in this article.

References

Aubele, J.C., Crumpler, L.S., Elston, W.E., 1988. Vesicle zonation and vertical structure of basalt flows. J. Volcanol. Geoth. Res. 35, 349–374. https://doi.org/10.1016/0377-0273(88)90028-5.

Baraff, D., Witkin, A., 1998. Large steps in cloth simulation. Computer Graphics Proceedings, Annual Conference Series 25, 43–54.

Beck, M.E., 1980. Paleomagnetic record of plate-margin tectonic processes along the western edge of North America. J. Geophs. Res. Solid Earth. 85 (B12), 7115–7131. https://doi.org/10.1029/JB085iB12p07115.

Bigi, S., Conti, A., Casero, P., Ruggiero, L., Recanati, R., Lipparini, L., 2013. Geological model of the central Periadriatic basin (Apennines, Italy). Mar. Petrol. Geol. 42, 107–121. https://doi.org/10.1016/j.marpetgeo.2012.07.005.

Blakely, R.J., Sherrod, B.L., Weaver, C.S., Wells, R.E., Rohay, A.C., Barnett, E.A., Knepprath, N.E., 2011. Connecting the Yakima fold and thrust belt to active faults in the Puget Lowland, Washington. J. Geophys. Res. 116, 1–33. https://doi.org/10.1029/2010JP008091.

Brocher, T.M., Wells, R.E., Lamb, A.P., Weaver, C.S., 2017. Evidence for distributed clockwise rotation of the crust in the northwestern United States from fault geometries and focal mechanisms. Tectonics 36 (5), 787–818. https://doi.org/10.1002/2016TC004223.

Camp, V.E., 2013. Origin of Columbia River Basalt: passive rise of shallow mantle, or active upwelling of a deep-mantle plume? In: Reidel, S.P., Camp, V.E., Ross, M.E., Wolff, J.A., Martin, B.S., Tolan, T.L., Wells, R.E. (Eds.), The Columbia River Basalt Province. vol. 497. Geol. S. Am. S., Boulder, CO, pp. 181–200. https://doi.org/10.1130/2013.2497(07).

Camp, V.E., Ross, M.E., 2004. Mantle dynamics and genesis of mafic magmatism in the intermontane Pacific Northwest. J. Geophys. Res. 109 (B8), 1–14. https://doi.org/10.1029/2003JB002838.

Campbell, N.P., 1989. Structural and stratigraphic interpretation of rocks under the Yakima fold belt, Columbia Basin, based on recent surface mapping and well data. In: Reidel, S.P., Hooper, P.R. (Eds.), Volcanic and Tectonism in the Columbia River Flood-Basalt Province. vol. 239. Geol. S. Am. S., Boulder, CO, pp. 209–222. https://doi.org/10.1130/SPE239-p209.

Caress, D.W., Menard, H.W., Hey, R.N., 1988. Eocene reorganization of the Pacific-Farallon spreading center north of the Mendocino Fracture Zone. J. Geophys. Res.–Sol. Ea. 93 (B4), 2813–2838. https://doi.org/10.1029/JB093iB04p02813.

Casale, G., Pratt, T.L., 2015. Thin- or thick-skinned faulting in the Yakima fold and thrust belt (WA)? Constraints from kinematic modeling of the saddle mountains anticline. B. Seismol. Soc. Am. 105 (2A), 745–752. https://doi.org/10.1785/0120140207.

Chan, C.F., Tepper, J.H., Nelson, B.K., 2012. Petrology of the Grays River volcanics, southwest Washington: plume-influenced slab window magmatism in the Cascadia forearc. Geol. Soc. Am. Bull. 124 (7–8), 1324–1338. https://doi.org/10.1130/B30576.1.

Cheney, E.S., 1994. Cenozoic unconformity-bounded sequences of central and eastern Washington. In: Washington Division of Geology and Earth Resources Bulletin. vol. 80. pp. 115–139.

Colgan, J.P., Henry, C.D., 2009. Rapid middle Miocene collapse of the Mesozoic orogenic plateau in north-central Nevada. Int. Geol. Rev. 51 (9–11), 920–961. https://doi.org/10.1080/00206810903056731.

Cowie, P.A., Scholz, C.H., 1992. Physical explanation for the displacement-length relationship of faults using a post-yield fracture mechanics model. J. Struct. Geol. 14 (10), 1133–1148. https://doi.org/10.1016/0191-8141(92)90065-5.

Crane, K.T., Klimczak, C., 2019. Tectonic patterns of shortening landforms in Mercury's northern smooth plains. Icarus 317, 66–88. https://doi.org/10.1016/j.icarus.2018.05.034.

Duncan, R.A., 1982. A captured island chain in the Coast Range of Oregon and Washington. J. Geophys. Res. 87, 10827–10837. https://doi:10.1029/JB087iB13p10827.

Eddy, M.P., Bowring, S.A., Umhoefer, P.J., Miller, R.B., McLean, N.M., Donaghy, E.E., 2016. High-resolution temporal and stratigraphic record of Siletzia's accretion and triple junction migration from nonmarine sedimentary basins in central and western Washington. Geol. Soc. Am. Bull. 128 (3/4), 425–441. https://doi.org/10.1130/B31335.1.

Gomberg, J., Sherrod, B., Trautman, M., Burns, E., Snyder, D., 2012. Contemporary seismicity in and around the Yakima fold-and-thrust belt in eastern Washington. B. Seismol. Soc. Am. 102 (1), 309–320. https://doi.org/10.1785/0120110065.

Graham, D.W., Reid, M.R., Jordan, B.T., Grunder, A.L., Leeman, W.P., Lupton, J.E., 2009. Mantle source provinces beneath the Northwestern USA delimited by helium isotopes in young basalts. J. Volcanol. Geoth. Res. 188 (1–3), 128–140. https://doi.org/10.1016/j.jvolgeores.2008.12.004.

Higgins, S., Davies, R.J., Clarke, B., 2007. Antithetic fault linkages in a deep water fold and thrust belt. J. Struct. Geol. 29 (12), 1900–1914. https://doi.org/10.1016/j.jsg.2007.09.004.

Kelsey, H.M., Ladinsky, T.C., Staisch, L., Sherrod, B.L., Blakely, R.J., Pratt, T.L., Stephenson, W.J., Odum, J.K., Wan, E., 2017. The story of a Yakima Fold and how it informs Late Neogene and Quaternary backarc deformation in the Cascadia Subduction Zone, Manastash Anticline, Washington, USA. Tectonics 36 (10), 2085–2107. https://doi.org/10.1002/2017TC004558.

Last, G.V., Winsor, K., Unwin, S.D., 2012. A Summary of Information on the Behavior of the Yakima Fold Belt as a Structural Entity: Topical Report. United States Department of Energy, Pacific Northwest National Labhttps://doi.org/10.2172/1053763.

Linnros, H., Hansman, R., Ring, U., 2019. The 3D geometry of the Naxos detachment fault and the three-dimensional tectonic architecture of the Naxos metamorphic core complex, Aegean Sea, Greece. 108 (1), 287–300. https://doi.org/10.1007/s00531-018-1654-2.

McCaffrey, R., King, R.W., Payne, S.J., Lancaster, M., 2013. Active tectonics of northwestern U.S. inferred from GPS-derived surface velocities. J. Geophys. Res.– Sol. Ea. 118 (2), 709–723. https://doi.org/10.1029/2012JB009473.

McCaffrey, R., King, R.W., Wells, R.E., Lancaster, M., Miller, M.M., 2016. Contemporary deformation in the Yakima fold and thrust belt estimated with GPS. Geophys. J. Int. 207, 1–11. https://doi.org/10.1093/gji/ggw252.

McCrory, P.A., Wilson, D.S., 2013. A kinematic model for the formation of the Siletz-Crescent forearc terrane by capture of coherent fragments of the Farallon and Resurrections plates. Tectonics 32, 718–736. https://doi:10.1002/tect.20045.

Moothart, S.R., 1992. Geology of the Middle and Upper Eocene McIntosh Formation and Adjacent Volcanic and Sedimentary Rock Units, Willapa Hillis, Pacific County, Southwest Washington. M.S. thesis. Oreg. State Univ., Corvallis, Oreg.

Morriss, M.C., Karlstom, L., 2018. The Chief Joseph Dike Swarm of the Columbia River Flood Basalts, and the Legacy Dataset of William H. Taubeneck. American Geophysical Union Annual Meeting. (abstract #V31H-0216).

Muir, R.J., 2017. Moving faults and building fracture models in a digital world – an example from Glen Coe, Scotland. Geol. Today 33 (2), 54–59. https://doi.org/10.1111/gto.12180.

Obrebski, M., Allen, R.M., Xue, M., Hung, S.H., 2010. Slab-plume interaction beneath the Pacific Northwest. Geophys. Res. Lett. 37 (14), 1–6. https://doi.org/10.1029/2010GL043489.

Perrouty, S., Lindsay, M.D., Jessell, M.W., Aillères, L., Martin, R., Bourassa, Y., 2014. 3D modeling of the Ashanti Belt, southwest Ghana: evidence for a litho-stratigraphic control on gold occurrences within the Birimian Sefwi Group. Ore Geol. Rev. 63, 252–264. https://doi.org/10.1016/j.oregeorev.2014.05.011.

Pratt, T., 2012. Large-scale splay faults on a strike-slip fault system: the Yakima Folds, Washington State. Geochem. Geophy. Geosy. 13 (11), 1–14. https://doi.org/10.1029/2012GC004405.

Provot, X., 1995. Deformation constraints in a mass-spring model to describe rigid cloth behavior. In: Graphics Interface. Canadian Information Processing Society.

Pyle, D.G., Duncan, R.A., Wells, R.E., Graham, D.W., Harrison, B., Hanan, B., 2009. Siletzia: an oceanic large igneous province in the Pacific Northwest. Geol. Soc. Am. Abstr. Prog. 41 (7), 369.

Reidel, S.P., 1984. The Saddle Mountains; the evolution of an anticline in the Yakima fold belt. Am. J. Sci. 284 (8), 942–978. https://doi:10.2475/ajs.284.8.942.

[dataset]Reidel, S.P., 1988. Geologic Map of the Saddle Mountains, South-Central Washington. Washington Division of Geology and Earth Resources: Geologic Map GM-38.

Reidel, S.P., Tolan, T.L., 2013. The late Cenozoic evolution of the Columbia River system in the Columbia River flood basalt province. In: Reidel, S.P., Camp, V.E., Ross, M.E., Wolff, J.A., Martin, B.S., Tolan, T.L., Wells, R.E. (Eds.), The Columbia River Basalt Province. vol. 497. Geol. S. Am. S., Boulder, CO, pp. 201–230. https://doi.org/10.1130/2013.2497(08).

Reidel, S.P., Martin, B.S., Petcovic, H.L., 2003. The Columbia River flood basalts and the Yakima fold belt. In: Swanson, T.W. (Ed.), Western Cordillera and Adjacent Areas. Geol. Soc. Am. Field Guide, Boulder, CO. vol. 4. pp. 87–105. https://doi.org/10.1130/0-8137-0004-3.87.

Reidel, S.P., Camp, V.E., Tolan, T.L., Martin, B.S., 2013. The Columbia River flood basalt province: stratigraphy, areal extent, volume, and physical volcanology. In: Reidel, S.P., Camp, V.E., Ross, M.E., Wolff, J.A., Martin, B.S., Tolan, T.L., Wells, R.E. (Eds.), The Columbia River Basalt Province. vol. 497. Geol. S. Am. S., Boulder, CO, pp. 1–44. https://doi.org/10.1130/2013.2497(01).

Schuster, J.E., 1994. Geologic Map of the east half of the Yakima 1:100,000 Quadrangle, Washington. Washington Division of Geology and Earth Resources: Open file report

94-12.
Sherrod, B.L., Blakely, R.J., Lasher, J.P., Lamb, A., Mahan, S.A., Foit, F.F., Barnett, E.A., 2016. Active faulting on the Wallula fault zone within the Olympic-Wallowa lineament, Washington State, USA. Geol. Soc. Am. Bull. 128 (11−12), 1636–1659. https://doi.org/10.1130/B31359.1.
Sheth, H., 2018. A Photographic Atlas of Flood Basalt Volcanism. Springer, Cham. https://doi.org/10.1007/978-3-319-67705-7_10.
Simpson, R.W., Cox, A., 1977. Paleomagnetic evidence for tectonic rotation of the Oregon Coast Range. Geology 5 (10), 585–589. https://doi:10.1130/0091-7613.
Snavely, P.D., MacLeod, N.S., Wagner, H.C., 1968. Theoleiitic and alkalic basalts of the Eocene Siletz River Volcanics, Oregon Coast Range. Am. J. Sci. 266, 454–481. https://doi:10.2475/ajs.266.6.454.
Staisch, L., Kelsey, H., Sherrod, B., Möller, A., Paces, J., Blakely, R., Styron, R., 2017. Miocene–Pleistocene deformation of the Saddle Mountains: implications for seismic hazard in central Washington, USA. Geol. Soc. Am. Bull. 130 (3–4), 411–437. https://doi.org/10.1130/B31783.1.
Staisch, L., Blakely, R., Kelsey, H., Styron, R., Sherrod, B., 2018. Crustal structure and Quaternary acceleration of deformation rates in central Washington revealed by stream profile inversion, potential field geophysics, and structural geology of the Yakima folds. Tectonics 37 (6), 1750–1770. https://doi.org/10.1029/2017TC004916.
Storti, F., Salvini, F., McClay, K., 1997. Fault-related folding in sandbox analogue models of thrust wedges. J. Struct. Geol. 19, 583–602. https://doi.org/10.1016/S0191-8141(97)83029-5.
Suppe, J., 1983. Geometry and kinematics of fault-bend folding. Am. J. Sci. 283 (7), 684–721. https://doi:10.2475/ajs.283.7.684.
Swanson, D.A., Wright, T.L., Hooper, P.R., Bentley, R.D., 1979. Revisions in Stratigraphic Nomenclature of the Columbia River Basalt Group. U.S. Geol. Surv. Bull. 1457–Gpp. 1–59. https://doi.org/10.3133/b1457G.
Swanson, D.A., Wright, T.L., Camp, V.E., Gardner, J.N., Helz, R.T., Price, S.M., Reidel, S. P., and Ross, M.E., 1980. Reconnaissance Geologic Map of the Columbia River Basalt Group, Pullman and Walla Walla Quadrangles, Southeast Washington and Adjacent Idaho: U.S. Geological Survey Miscellaneous Investigations Series Map I-1139, scale 1:250,000, 2 sheets.
Tabor, R.W., Frizzell, V.A., Vance, J.A., Naeser, C.W., 1984. Ages and stratigraphy of lower and middle Tertiary sedimentary and volcanic rocks of the central Cascades, Washington: application to the tectonic history of the Straight Creek fault. Geol. Soc. Am. Bull. 95 (1), 26–44. https://doi.org/10.1130/0016-7606(1984)95<26:AASOLA>2.0.CO;2.
Terzopoulous, D., Platt, J., Barr, A., Fleischer, K., 1987. Elastically deformable models. Computer Graphics Proceedings, Annual Conference Series 21 (4), 205–214.
Tolan, T.L., Martin, B.S., Reidel, S.P., Anderson, J.L., Lindsey, K.A., Burt, W., 2009. An introduction to the stratigraphy, structural geology, and hydrogeology of the Columbia River Flood-Basalt Province: a primer for the GSA Columbia River Basalt Group field trips. Geol. Soc. Am. Field Guides. 15, 599–643. https://doi.org/10.1130/2009.fld015(28).
United States Geological Survey, 2006. Quaternary fault and fold database for the United States. http//earthquake.usgs.gov/hazards/qfaults/.
United States Geological Survey, 2010. Modeled Combined Extent of All Columbia River Basalt Units. Water Resources NSDI Node. https://water.usgs.gov/GIS/metadata/usgswrd/XML/sir2010-5246_CRB_extent4xconnections.xml.
Unruh, J., Humphrey, J., 2017. Seismogenic deformation between the Sierran microplate and Oregon Coast block, California, USA. Geology 45 (5), 415–418. https://doi.org/10.1130/G38696.1.
Wang, Y., Xiong, Y., Xu, K., Tan, K., Guo, G., 2006. A mass-spring model for surface mesh deformation based on shape matching. In: Proceedings of the 4th International Conference on Computer Graphics and Interactive Techniques in Australasia and Southeast Asia, pp. 375–380.
Washington Geological Survey, 2017. Surface geology, 1:24,000–GIS data, September 2017: Washington Geological Survey Digital Data Series DS-10, version 3.0. previously released November 2016. .
Watkins, H., Bond, C.E., Butler, R.W.H., 2014. Identifying multiple detachment horizons and an evolving thrust history through cross-section restoration and appraisal in the Moine Thrust Belt, NW Scotland. J. Struct. Geol. 66, 1–10. https://doi.org/10.1016/j.jsg.2014.05.001.
Wells, R.E., Heller, P.L., 1988. The relative contribution of accretion, shear, and extension, to Cenozoic tectonic rotation in the Pacific Northwest. Geol. Soc. Am. Bull. 100, 325–338. https://doi.org/10.1130/0016-7606(1988)100<0325:TRCOAS>2.3.CO;2.
Wells, R.E., McCaffrey, R., 2013. Steady rotation of the Cascade arc. Geology 41 (9), 1027–1030. https://doi.org/10.1130/G34514.1.
Wells, R.E., Engebretson, D.C., Snavely, P.D., 1984. Cenozoic plate motions and the volcano-tectonic evolution of western Oregon and Washington. Tectonics 3 (2), 275–294. https://doi.org/10.1029/TC003i002p00275.
Wells, R.E., Snavely, P.D., MacLeod, N.S., Kelly, M.M., and Parker, M.J., 1994. Geologic Map of the Tillamook Highlands, Northwest Oregon Coast Range (Tillamook, Nehalem, Enright, Timber, Fairdale, and Blain 15-minute quadrangles), scale 1:62,500. U.S. Geol. Surv. Open-File Rep. 94–21.
Wells, R.E., Jayko, A.S., Niem, A.R., Black, G., Wiley, T., Baldwin, E., Molenaar, K.M., Wheeler, K.L., DuRoss, C.B., Givler, R.W., 2000. Geologic map and database of the Roseburg 30 × 60′ Quadrangle, Douglas and Coos Counties, Oregon. In: U.S. Geol. Surv. Open-File Rep. 00–376, pp. 55.
Wells, R., Bukry, D., Friedman, R., Pyle, D., Duncan, R., Haeussler, P., Wooden, J., 2014. Geologic history of Siletzia, a large igneous province in the Oregon and Washington Coast Range: correlation to the geomagnetic polarity time scale and implications for a long-lived Yellowstone hotspot. Geosphere 10 (4), 692–719. https://doi.org/10.1130/GES01018.1.
West, M.W., Ashland, F.X., Busacca, A.J., Berger, G.W., Shaffer, M.E., 1996. Late Quaternary deformation, Saddle Mountains anticline, south-central Washington. Geology 24 (12), 1123–1126. https://doi.org/10.1130/0091-7613(1996)024<1123:LQDSMA>2.3.CO;2.
Wilson, D.S., 1988. Tectonic history of the Juan de Fuca Ridge over the last 40 million years. J. Geophys. Res.– Sol. Ea. 93 (B10), 11863–11876. https://doi.org/10.1029/JB093iB10p11863.
Yan, D.P., Xu, Y.B., Dong, Z.B., Qiu, L., Zhang, S., Wells, M., 2016. Fault-related fold styles and progressions in fold-thrust belts: insights from sandbox modeling. J. Geophys. Res.– Sol. Ea. 121 (3), 2087–2111. https://doi.org/10.1002/2015JB012397.